LAWRENCE
LIVERMORE
NATIONAL
LABORATORY

LLNL-JRNL-402708

Iron-Based Amorphous Coatings Produced by HVOF Thermal Spray Processing-Coating Structure and Properties

M.B. Beardsley

April 4, 2008

Metallurgical and Materials Transactions

Disclaimer

This document was prepared as an account of work sponsored by an agency of the United States government. Neither the United States government nor Lawrence Livermore National Security, LLC, nor any of their employees makes any warranty, expressed or implied, or assumes any legal liability or responsibility for the accuracy, completeness, or usefulness of any information, apparatus, product, or process disclosed, or represents that its use would not infringe privately owned rights. Reference herein to any specific commercial product, process, or service by trade name, trademark, manufacturer, or otherwise does not necessarily constitute or imply its endorsement, recommendation, or favoring by the United States government or Lawrence Livermore National Security, LLC. The views and opinions of authors expressed herein do not necessarily state or reflect those of the United States government or Lawrence Livermore National Security, LLC, and shall not be used for advertising or product endorsement purposes.

Iron-Based Amorphous Coatings Produced by HVOF Thermal Spray Processing – Coating Structure and Properties

M. Brad Beardsley
Ondrej Racek

Caterpillar Inc., Peoria, IL, USA,

Keywords: coatings, corrosion resistance, iron-based amorphous materials, high-velocity oxygen fuel, HVOF

Abstract

The feasibility to coat large SNF/HLW containers with a structurally amorphous material (SAM) was demonstrated on sub-scale models fabricated from Type 316L stainless steel. The sub-scale model were coated with SAM 1651 material using kerosene high velocity oxygen fuel (HVOF) torch to thicknesses ranging from 1 mm to 2 mm. The process parameters such as standoff distance, oxygen flow, and kerosene flow, were optimized in order to improve the corrosion properties of the coatings. Testing in an electrochemical cell and long-term exposure to a salt spray environment were used to guide the selection of process parameters.

Introduction

Some amorphous materials exhibit excellent corrosion resistance due to the absence of grain boundaries and homogeneous chemistry. Although there are some chemistries, such as $Zr_{41.2}Ti_{13.8}Cu_{12.5}Ni_{10}Be_{22.5}$ where the amorphous form provides little or no improvement over a crystalline material of the same chemistry [1], the statement holds true for a class of iron-based amorphous alloys [2]. An example of iron-based amorphous alloy is SAM 1651, $Fe_{48}Cr_{15}Mo_{14}B_6C_{15}$. If the melt is cooled at a rate higher than the critical cooling rate amorphous structure is formed. Low critical cooling rate is characteristic for SAM 1651, which makes it possible to produce amorphous material by gas atomization in a form of powder or even drop-cast ingots several millimeters in diameter [3]. Powder feedstock may be used to produce coatings using a thermal spray process.

Thermal spray is used to deposit coatings of materials ranging from polymers [4], metals [5], to ceramics [6] on dissimilar substrates. A variety of thermal spray methods is used or investigated such cold spray, arc spray, plasma spray, or high-velocity oxygen fuel (HVOF). HVOF uses a mixture of fuel and oxygen that is combusted and accelerated through a nozzle and barrel. Feedstock powder is injected in the barrel where it is heated and accelerated to supersonic velocity. Due to the high velocity and relatively low temperature of the gas, approximately below 3000C, the conditions can be set such that the feedstock is only partially melted or softened. Lower temperature and short residential times cause less change in the material chemistry, carbon loss in a commonly used WC-Co type material was determined to be 25-70% depending on the type of torch used [7]. Particle resident time in the flame is in order of millisecond and the splat cooling rate after an impact on a substrate in order of $10^7 C.s^{-1}$ [8]. Thermal spray process is capable of producing amorphous structure [9] either because no re-crystallization takes place during the short particle resident time or splats cool faster than the critical cooling rate, which is about 610 $K.s^{-1}$ [10]. HVOF process was used to deposit an amorphous material,

SAM 1651, in the present study. Low porosity, comparable to vacuum plasma spray (VPS), can be achieved using HVOF.

Previously, containers in 1:2 scales were coated with 1 to 2 mm thick coating. The 316 stainless steel container was cylindrical about 762 mm (30”) in diameter and about 2235.2 mm (88”) long. The surface of the initial thick coating samples were rough and contained “speckles”, Figure 1a, b. It was noticed that the coating roughness increased with increasing thickness. The coating roughness was also lower close to the edges of samples, Figure 1c. Subsequent corrosion testing revealed that the speckles are quickly attacked by corrosion due to presence of porosity, Figure 2. The speckles of porosity had a conical shape starting from a layer close to the coating/substrate interface, Figure 3.

It was discovered that a feedstock with larger particle size did not produce the speckles under the same deposition conditions, Figure 4. Powder lot #130661 was produced during the development of the atomization process and contained higher number of large particles than the other powder lots used such as lot# V5793, Figure 5. Particle size was measured using a laser light scattering method and clearly showed a shift in the average particle size of lot #130661 compared to other powder lots, Figure 6. The coating made with #130661 powder lot; however, did not exhibit a significantly better corrosion behavior and spots of rust were produced within 120 hours of salt spray testing per ASTM B117, Figure 7. Coating surface morphology changed; however, it appears that overall coating microstructure was not improved, i.e. significant amount of porosity was still present. This perception of coating porosity was in agreement with the hardness data, which is a function of porosity [11, 12]. Higher density results in a higher hardness. The hardness of the speckled coating was 731HV(300g)±91 and the coating deposited with larger particle size feedstock 683HV(300g)±140.

It appeared from the speckle morphology, its high porosity, and high oxide content that the mechanism that causes the speckles to occur is related to small droplets that are produce either by splashing or fracturing of impacting particles. It was also considered that small particles in the feedstock might be deflected in the jet streamlines as it impinges on the substrate. The small particles would then travel on a trajectory that is more parallel to the surface and could deposit on any coating surface perturbation. As the coating thickness is built up, the perturbations would grow as well presenting a larger cross-sectional area for the particles to deposit on, Figure 8. A similar mechanism has been described for a plasma sprayed alumina [13]; it was suggested that the perturbation morphology contributes to splashing of primary particles.

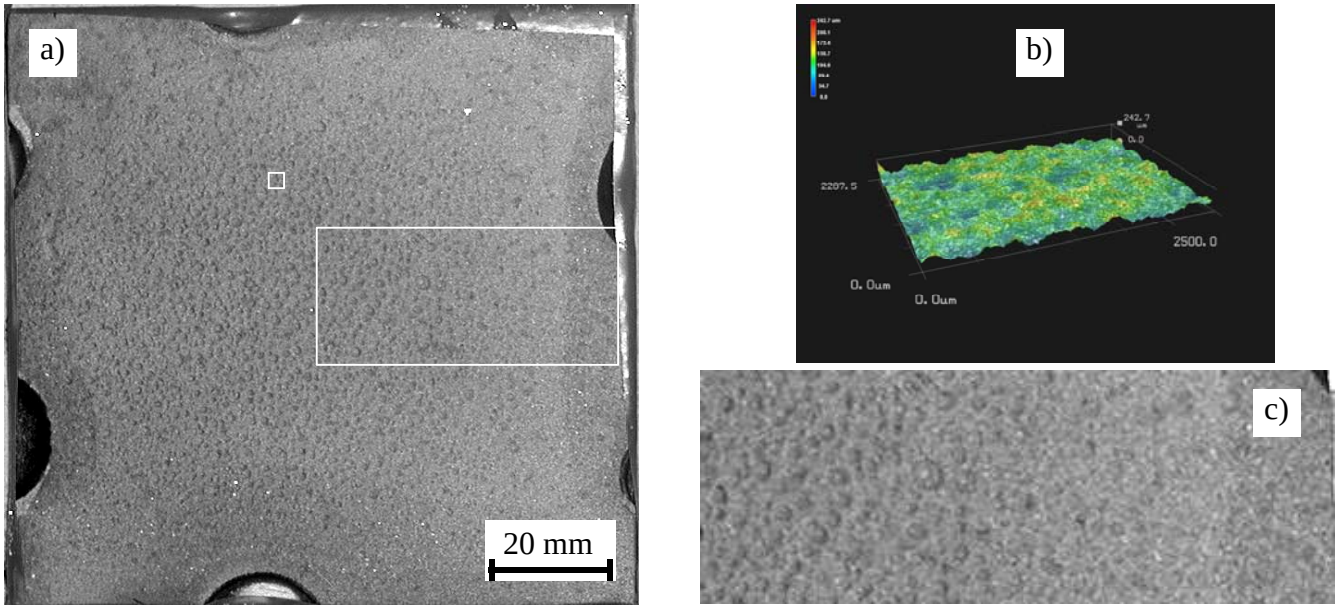

Figure 1 a) a 316 stainless steel panel coated with initial SAM 1651 coating, b) 3-D map of the surface, c) surface roughness gradient close to the edge of the coating

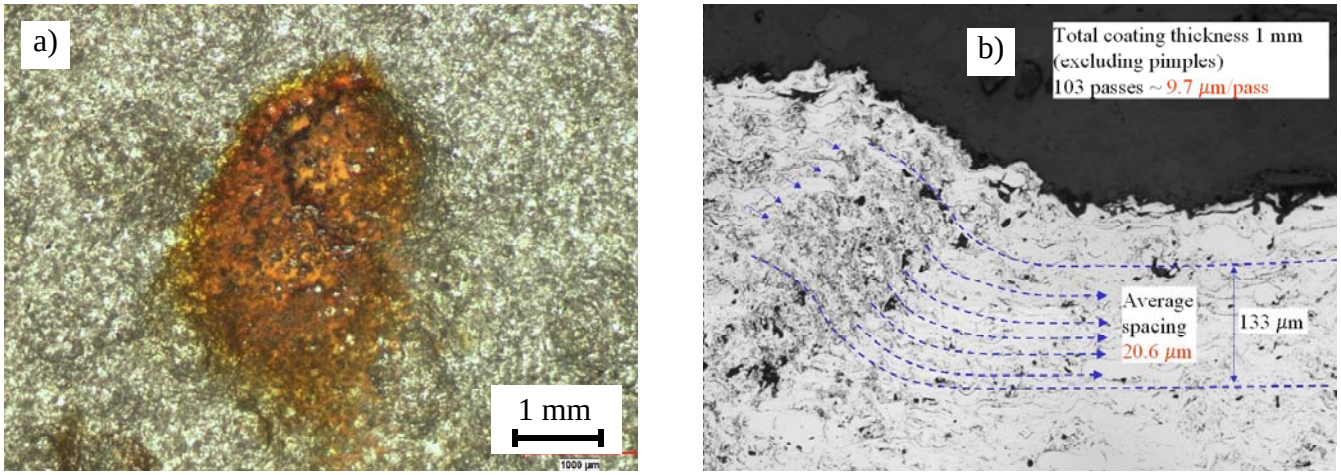

Figure 2 One of the initial SAM 1651 coatings; a) a corroded speckle on the coating surface, b) cross-section of a speckle

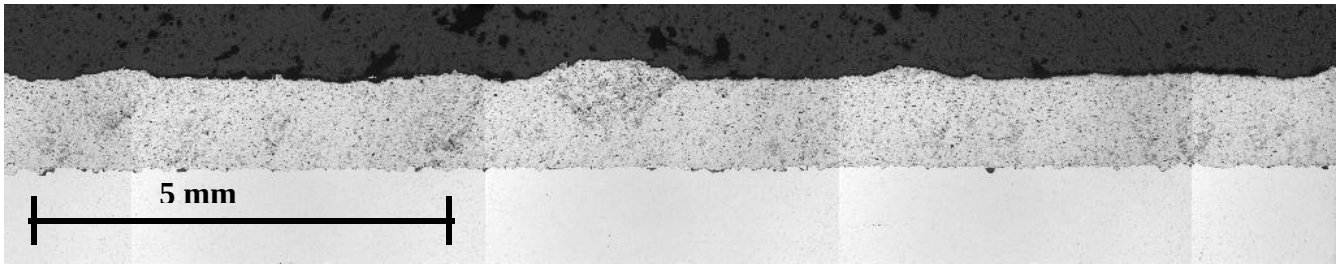

Figure 3 A speckle microstructure in the specimen 06-0925-E-1 (V5793 powder lot#)

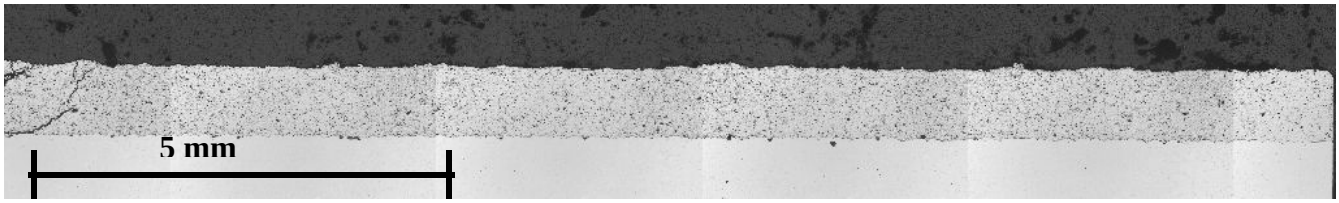

Figure 4 Microstructure of the speckle-free sample 06-0923-E-1 (130661 powder lot#)

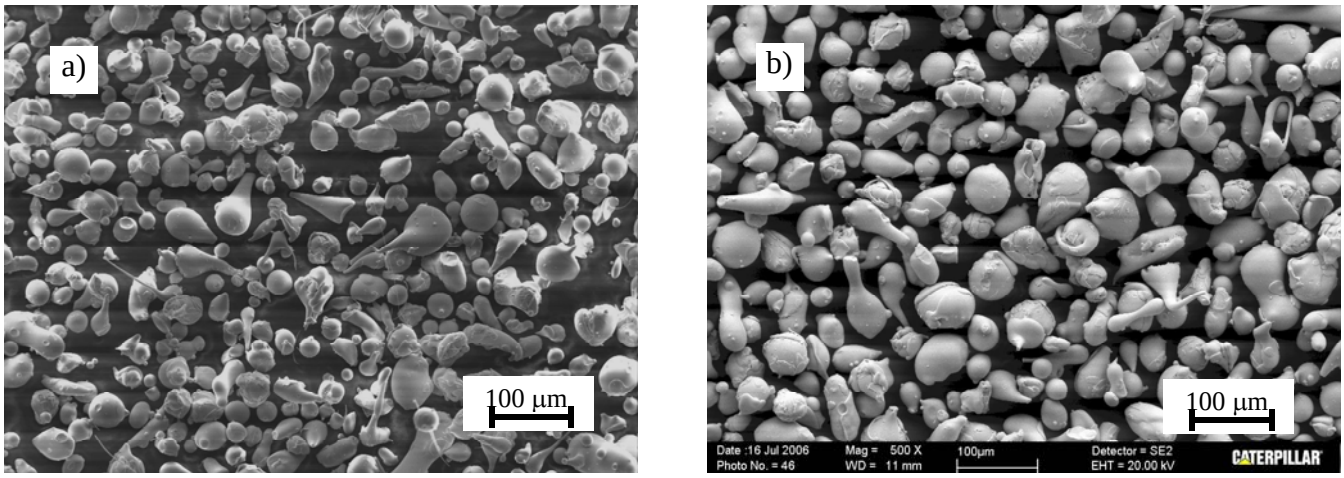

Figure 5 a) SAM 1651 V5793 powder lot, b) 130661 powder lot#

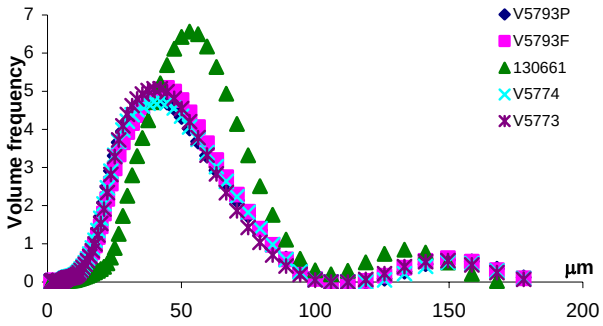

Figure 6 Particle size distribution (laser particle size analyzer) of SAM 1651 powder lots used for qualifications samples and/or sub-scale package model

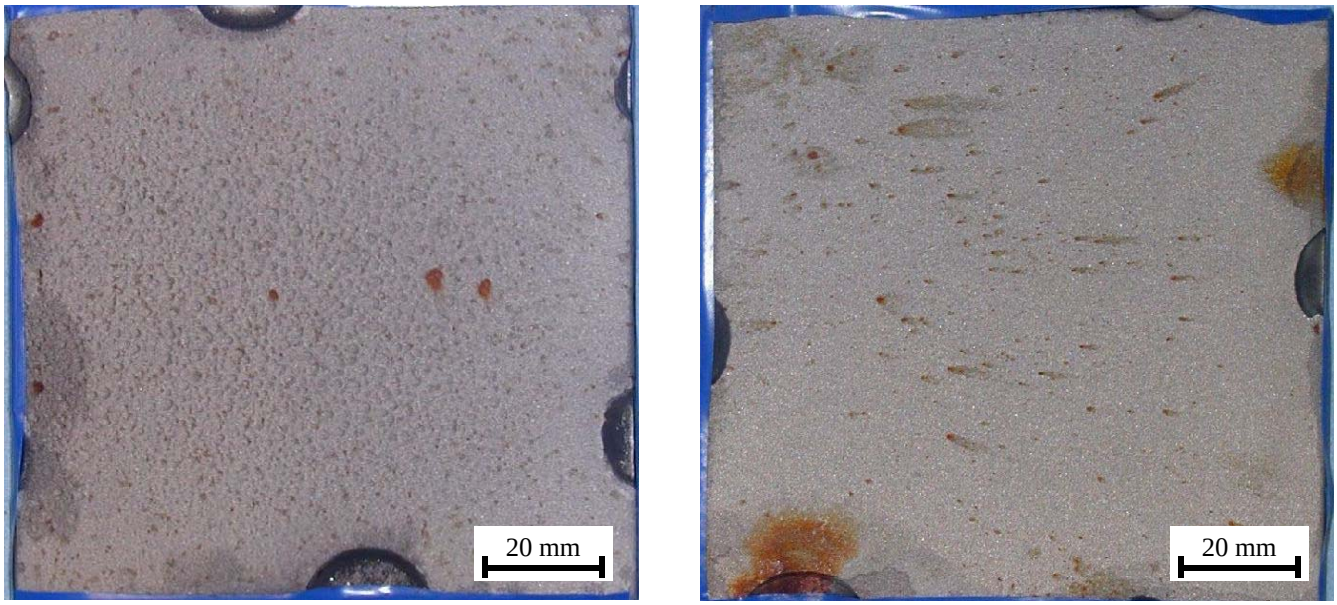

Figure 7 Salt spray tested (120 hours) coatings produced with a) SAM 1651 V5793 powder lot, b) larger particle size 130661 powder lot#

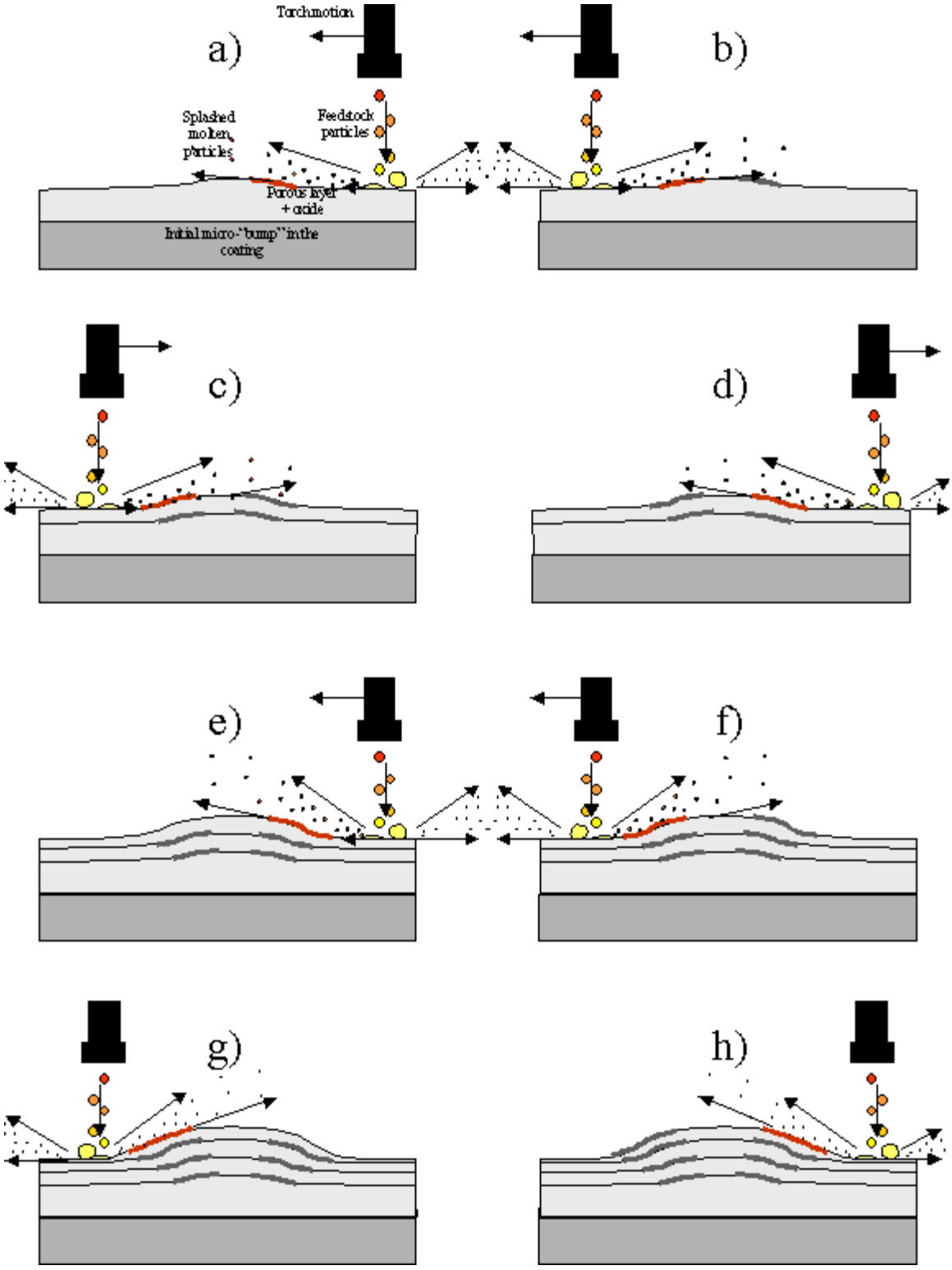

Figure 8 The suggested relationship of the oxide/porosity layers and the torch motion

Materials and Processes

Coating deposition

Coatings were deposited using a JP 5000 (Praxair Surface Technologies TAFA Incorporated, Concord, NH, USA) kerosene torch. Fuel and oxygen is mixed in a combustion chamber, simplified cross-section in Figure 9, the hot gases exit through a short diverging nozzle into an inter-connector that is followed by a barrel. Powder feedstock is injected in the inter-connector section just prior to the barrel. Barrels of two different lengths were used, 101.6 mm (4") and 152.4 mm (6").
The torch was mounted on a robot. To produce a uniform coating on flat panels, the torch was moved over substrates in a raster pattern. The motion parameters were the same for all specimens, 1000 mm/s speed and 6 mm distance between raster lines. The HVOF process parameters investigated in the present study are listed in Table 1. The standoff distance is measured from the outlet of the barrel. The distance the powder feedstock travels from where it is injected to the flame to the substrate is a sum of the standoff and the barrel length.

In-flight particle temperature and velocity measurement

DPV2000 (Tecnar Automation Ltée, St-Bruno, QC, Canada) was used for measurement of particle speed and velocity in the hot flame. The measurement is based on analyzing a signal that originates from a single particle. A single particle generates a two-peak signal as it passes through two small volumes that are defined by two slits placed in front of the lenses. The volumes are small so there is a high chance that only a single particle enters them in a single measurement time window. From the distance between the volumes and the time between the two peaks, the velocity is calculated. Infrared sensor is used to detect the signal and the temperature measurement is based on two-color pyrometry.

Corrosion testing

Coating samples were tested in an electrochemical cell with a Ag/AgCl reference electrode in 5M $CaCl_2$ solution at 105°C and in ASTM D1141 salt water solution at 90°C. Cyclic polarization was performed on as-deposited coatings to evaluate the resistance to localized corrosion. Hastelloy C-22 and stainless 316 alloys were used as baseline specimens. Coatings were also tested in a salt spray environment according to ASTM B117 standard. A tape protected the uncoated sides of the specimens. The test results were used to guide the selection of process parameters and were not intended to predict the material lifetime in a long term.

Results

To investigate the mechanism that causes the speckle formation within a coating, individual splats were deposited on polished stainless steel substrates and studied using a scanning electron microscopy (SEM). The torch was passed at a relatively high speed of 2000 mm/s over a polished steel substrate that had a 6 mm step. The particles deposited on the surface perpendicular to the torch axis were observed as well as the particles deposited on the surface of the step parallel to the torch axis, Figure 10a). A thin layer was built up on the parallel surface, Figure 10b), that could have been a result of either small particles deviated along the gas streamlines before the impact or splashed particles after the impact. The particles that were deposited on the perpendicular surface exhibited irregular shapes

and were covered with small droplets that are believed to originate from splashing of the primary particles on impact, Figure 10c). Some particles were deposited on top of particles that arrived earlier and these “fresh” particles were covered with significantly less droplets. A closer inspection of the coating on the parallel surface, Figure 10d), revealed that the material consists of small particles less than 10 μm in diameter. It is suggested that these particles originate from splashing of primary particles and play the key role in the formation of porous speckles within the coating, Figure 2. It is unlikely that the small particles come from a small-diameter fraction of the powder feedstock since there are very few particles under 10 μm in diameter, Figure 5 and Figure 6.

Splashing behavior is controlled by both the velocity and temperature, which is consistent with Sommerfeld parameter used to describe the particle impact mode in plasma spray [14]:

$$K = \frac{\rho^{\frac{3}{4}} \cdot d^{\frac{3}{4}} \cdot v^{\frac{5}{4}}}{\sigma^{\frac{1}{2}} \cdot \mu^{\frac{1}{4}}} \tag{1}$$

where ρ is the particle density, d diameter, v velocity, σ surface tension, and μ viscosity. This equation has been used for fully molten particles in plasma spray. In HVOF deposition the particles are typically not liquid however the SAM materials exhibit a viscous behavior over the glass transition temperature of about 580 C [2].

The particle velocities and temperatures were studied at various standoff distances torch settings listed in Table 1. The particle speed declines significantly with increasing standoff distance, Figure 11. The particle temperature appears to increase slightly with increasing standoff. It should be noted that the measured particle temperature relates directly only to the particle surface.

Shorter standoff distance results in a lower particle surface temperature and shorted resident times, which may suggest that the particles are less melted and would splash less on impact. It was found, however, that shorter standoff resulted in a more speckled coating, Figure 12, which suggests that more splashing occurred. This result seems to agree to direct observation of individual splats deposited on a polished steel substrate, Figure 13; however, no quantitative evaluation of the amount of splashed material was done.

The in-flight particle measurements suggested that a use of 152.4 mm (6”) barrel length at lower fuel and oxygen flows results in similar velocities compared to torch with a 101.6 mm (4”) barrel length; however, the particle surface temperature is lower, Figure 11. Coatings deposited with a shorter barrel exhibited speckles on the surface at standoff distances shorter than 355.6 mm (14”). A coating deposited with a longer barrel at 304.8 mm (12”) standoff, where the velocity is similar to a shorter barrel and the same standoff, did not exhibit speckles but the coating surface became rough at standoff distance 254 mm (10”). This result is in agreement with the equation (1); a condition with a higher velocity can result in the same Sommerfeld parameter if decreasing the temperature increases the viscosity accordingly.

No significant difference was observed in microstructures of the coatings that did not exhibit speckles. A microstructure of a coating deposited with a shorter barrel, at oxygen flow of 840 slpm and 23.9 lph kerosene flow, is representative of “smooth” coatings deposited with other torch parameters, Figure 14. However, the corrosion properties of the coatings measured using an electrochemical cell were quite different, Figure 15. The coating deposited with a shorter barrel, 840 slpm oxygen flow and 23.9 lph kerosene flow exhibited higher difference between the corrosion potential E_{corr} and the critical potential, E_p, or the re-passivation potential, E_{rp}, Table 2. Passive film breakdown occurs at the critical

potential and the larger the difference between corrosion potential and the critical potential the higher the resistance to localized corrosion [10].

The surface of the coating corroded during the electrochemical test in $CaCl_2$ at 105C was examined using SEM. Corrosion pits were observed on the surface of splats; however, the coating appears to be attacked primarily at the splat edges and splat-splat interfaces, Figure 16.

Salt spray testing confirmed that the coatings deposited with speckles on the surface, shorter standoff distances at a given torch setting, exhibit a poor corrosion resistance, Figure 17. The coating deposited with a shorter barrel and 840 slpm oxygen flow did not exhibit any signs of corrosion attack in the area further from the edges of the masking tape Figure 17b. Within 408 hours of test a few spots attacked by corrosion appeared on the coating deposited with a shorter barrel and 768 slpm oxygen flow, Figure 17d. Although the coating deposited with a longer barrel at 304.8 mm standoff did not contain any speckles, the surface exhibited a significant amount of corrosion within 312 hours of test, Figure 17f. The surface of the best performing coating did not contain signs of corrosion after a further testing at 1416 hours when the salt spray test was stopped, Figure 18a.

Table 1 Selected JP 5000 parameters for SAM 1651 feedstock

O2 flow	Kerosene flow	Feed rate	N2 carrier flow	Barrel length	Standoff
slpm	Lph	g/min	slpm	mm	(mm)
768	23.9	76	10.5	101.6	304.8
768	23.9	76	10.5	101.6	330.2
768	23.9	76	10.5	101.6	355.6
840	23.9	76	10.5	101.6	304.8
840	23.9	76	10.5	101.6	330.2
840	23.9	76	10.5	101.6	355.6
739	21.8	76	9.5	152.4	254.0
739	21.8	76	9.5	152.4	279.4
739	21.8	76	9.5	152.4	304.8

Table 2 Summary of electrochemical test of SAM 1651 coatings in $CaCl_2$ at 105C

Material	Thickness (mm)	**Ecorr (mV)**	**Ep (mV)**	**Ip (μA/cm2)**	**Erp (mV)**	**ΔE=Erp-Ecorr (mV)**
SAM1651, 840/23.9, 4" barrel, 14" SOD	**1**	-136	303	2	65	201
SAM1651, 768/23.9, 4" barrel 14" SOD	**1**	-100	224	140	-8	92
SAM1651, 739/21.8, 6" barrel 12" SOD	**0.2**	-336	211	719	-268	68
SAM1651, 739/21.8, 6" barrel 12" SOD	**1**	-343	200	1684	-228	115
316L	**-**	-337	-252	12.1	-330	7
C22	**-**	-260	80	4	-173	87
SAM1651[2] drop cast ingot	**-**	-180	250	30	300	480
SAM1651[15] drop cast ingot	**-**	-300	350	7	250	550

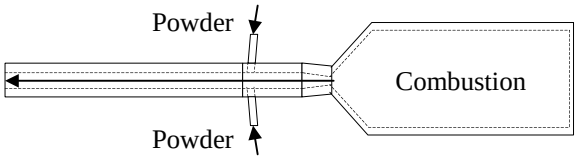

Figure 9 Simplified cross-section of the JP 5000 torch

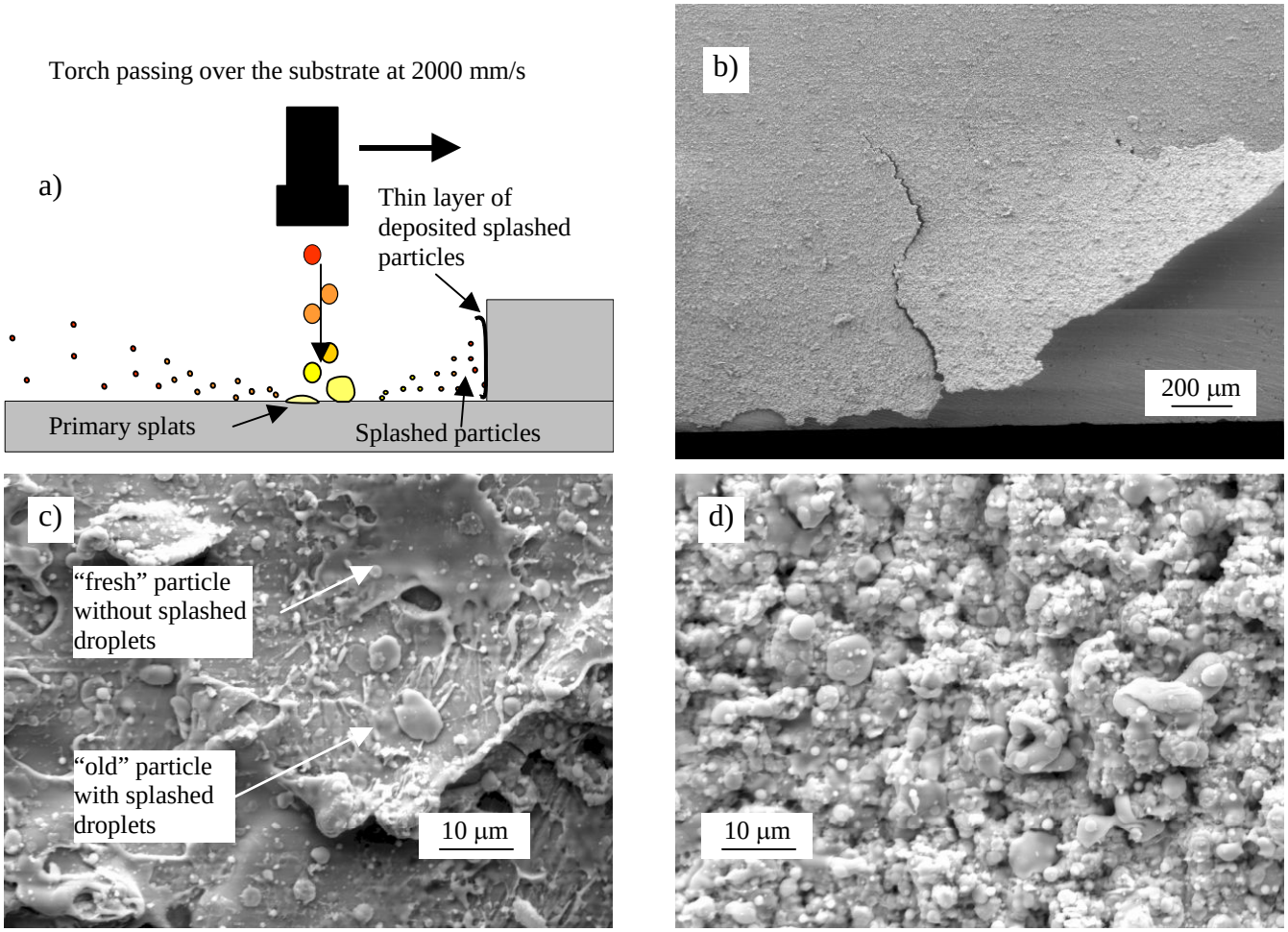

Figure 10 Splashing of impacting semi-molten particles (840 slpm oxygen, 23.9 lph kerosene at 12" standoff); a) experimental setup, b) thin layer of splashed particles deposited on the vertical surface, c) primary splat morphology with splashed droplets, d) a detail view of deposited splashed particles

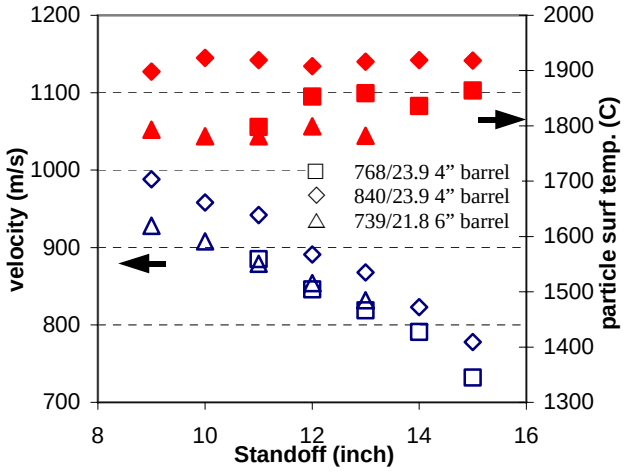

Figure 11 Comparison of average in-flight particle parameters for several runs tested for corrosion resistance

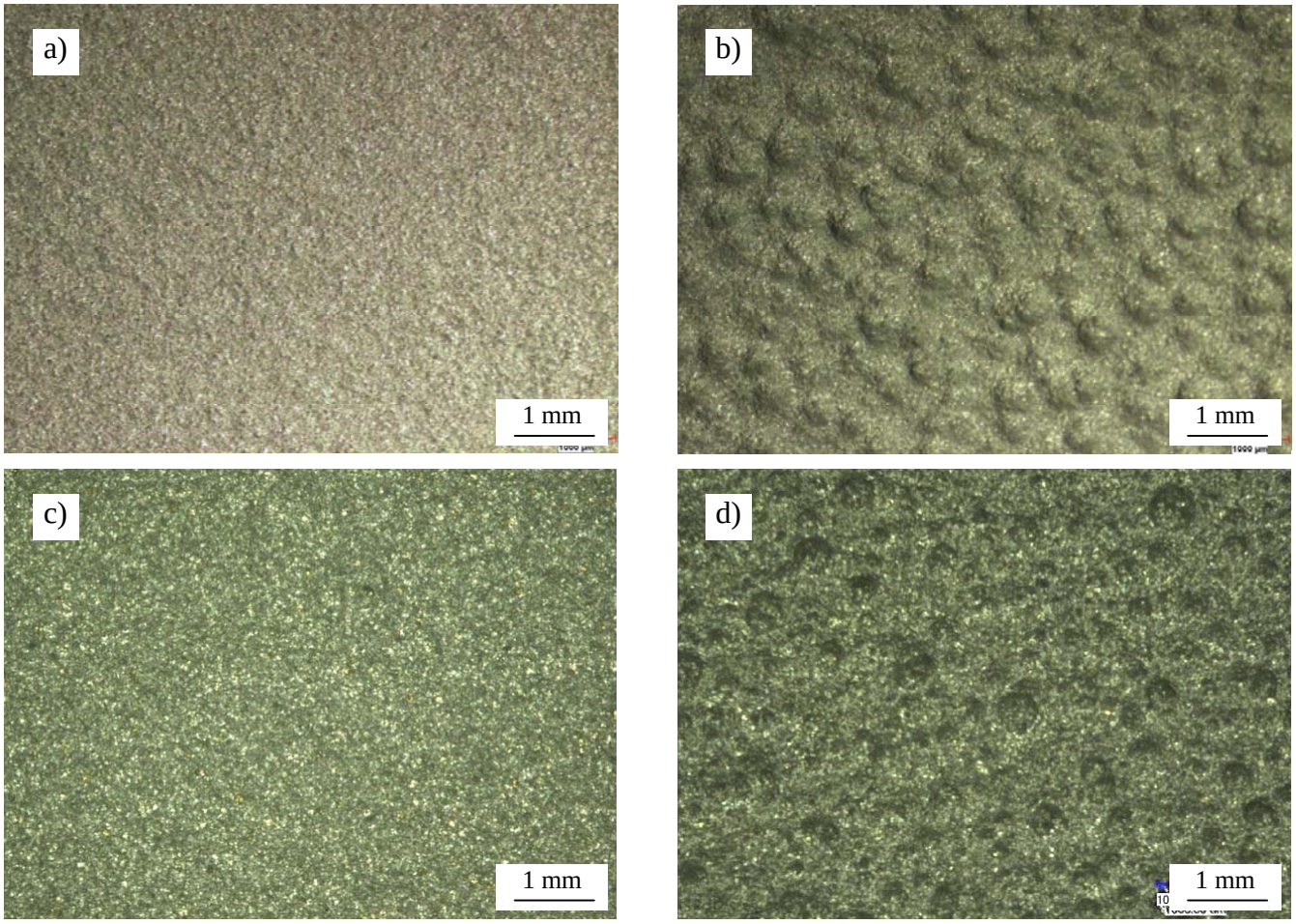

Figure 12 Surface morphology of SAM 1651 coating deposited with parameters; a) 840/23.9, 6” barrel, 14 “ standoff, b) 840/23.9, 6” barrel, 12” standoff, c) 739/21.8, 6” barrel, 12” standoff, d) 739/21.8, 6” barrel, 10” standoff

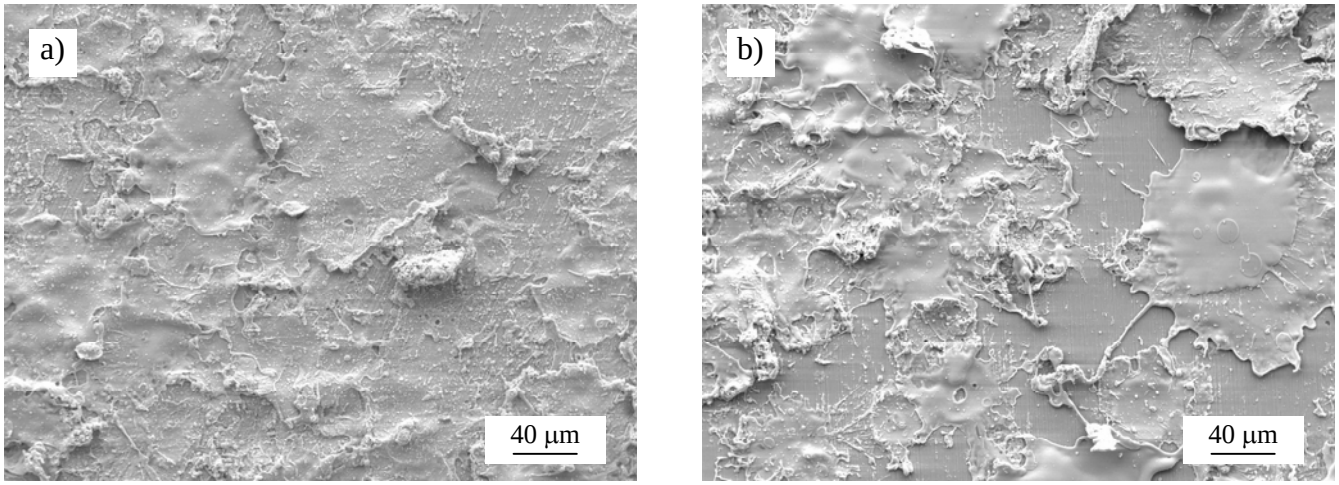

Figure 13 Morphology of SAM 1651 splats deposited with 4” barrel, 840 slpm oxygen, 23.9 lph kerosene: a) 12” standoff, b) 14” standoff

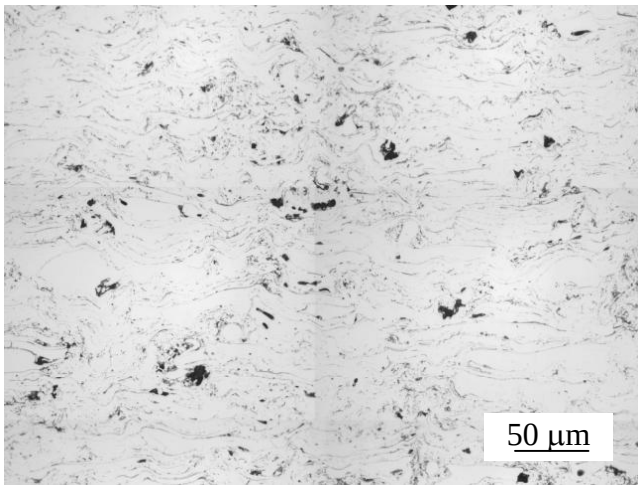

Figure 14 Microstructure of a coating deposited at 840 slpm oxygen flow, 23.9 lph kerosene flow, 14" standoff distance

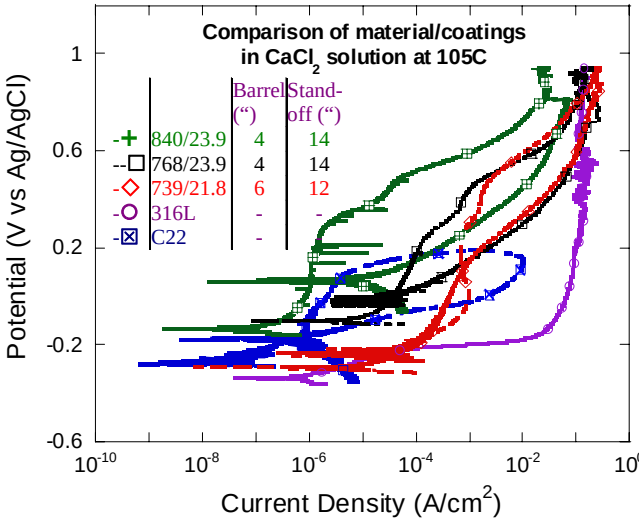

Figure 15 Polarization curves of SAM 1651 coatings (V5913) deposited with various parameters and comparison with 316 stainless and C-22

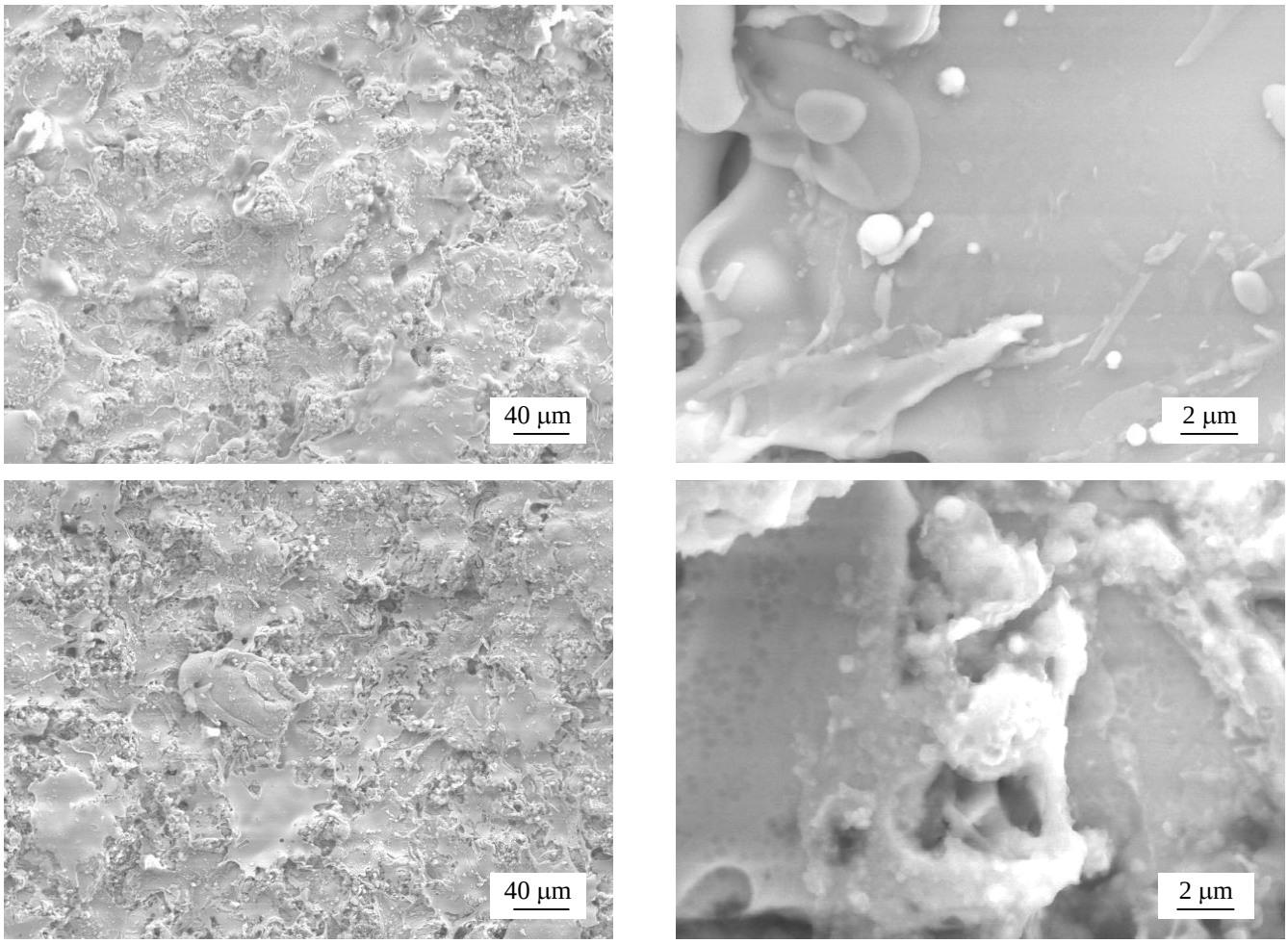

Figure 16 SAM 1651 coating deposited with 840/23.9 parameter at 14" standoff; a) as sprayed surface, b) surface after polarization test in $CaCl_2$ at 105°C

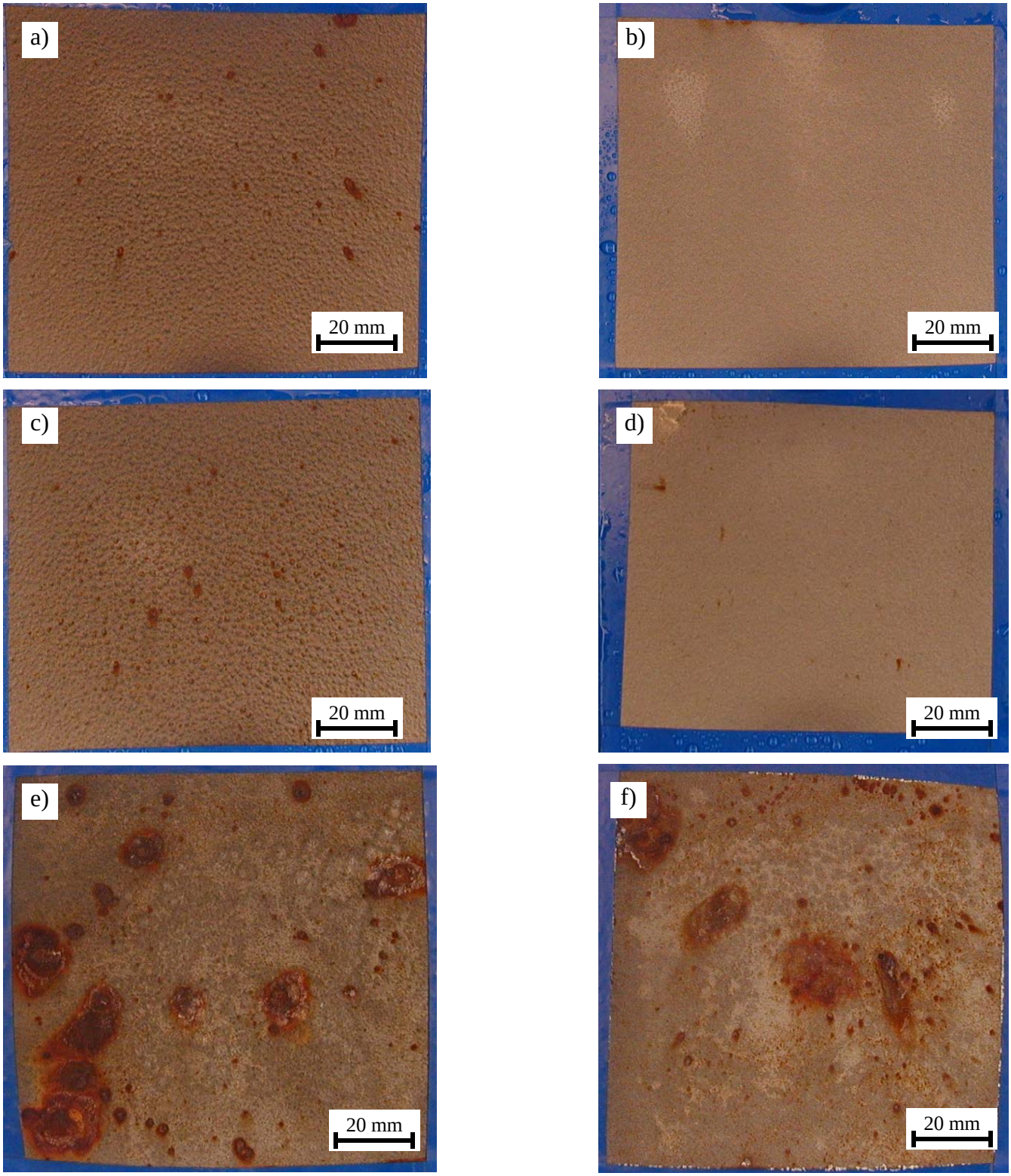

Figure 17 SAM 1651 coating samples after a salt spray exposure: 408 hour test, coating deposited with 840 slpm oxygen flow and 23.9 lph kerosene flow, 4" barrel at a) 12" standoff, b) 14" standoff; 771 slpm oxygen flow and 23.9 lph kerosene flow at c) 12" standoff, d) 14" standoff; 312 hour test, coating deposited with 739 slpm oxygen flow and 21.8 lph kerosene flow, 6" barrel at e) 10" standoff, f) 12" standoff

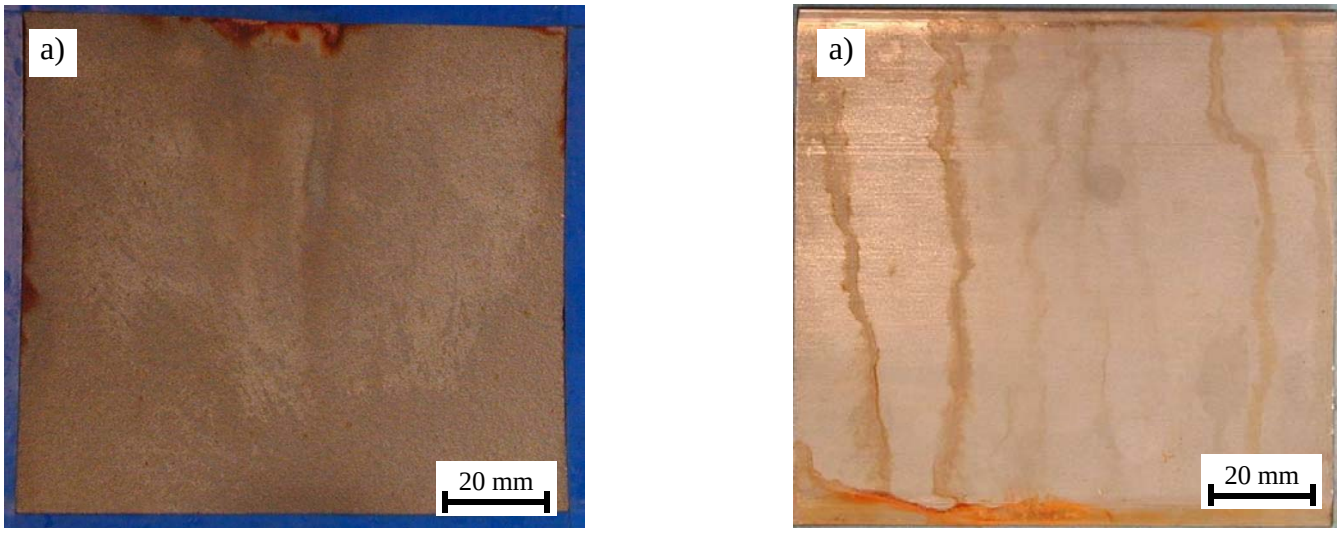

Figure 18 Surfaces of specimens after a salt spray test a) SAM 1615 coating, 840 slpm oxygen flow and 23.9 lph kerosene flow at 14" standoff distance (1416 hours), b) 316 stainless (1032 hours),

Discussion

The nature of the particles deposited on a surface parallel to the spray direction suggests that they originate from splashed primary particles. Longer standoff distances result in lower particle speed while a use of a longer barrel and lower oxygen and fuel flows results in similar particle velocities but a lower particle temperature. Deposition conditions can be set such that the particle velocity and temperature, and consequently amount of melted phase and/or viscosity, are balanced and coating can be deposited without speckles. There is strong evidence that the speckle appearance in the HVOF deposited SAM alloys is due to splashing of the impacting feedstock particles.

Corrosion resistance of a HVOF coating is a function of its microstructure due to the presence of imperfections such as splat boundaries or porosity. The coating is primarily attacked at these imperfections. Therefore speckle-free coating is not the only condition for a high corrosion resistance. High coating density and integrity needs to be achieved. Evaluation of coating microstructure using standard metallographic procedures is not sufficient to predict corrosion resistance of coatings since there was no significant difference in observed microstructure between coatings that performed differently in electrochemical testing. Electrochemical test results correlated well with the results of the salt spray test.

Speckle-free coatings were deposited both with a 101.6 mm and 152.4 mm barrels. The conditions using a longer barrel implied a lower particle temperature but higher velocity. The coatings deposited with a longer barrel performed poor in the corrosion test. It appears that the higher velocity did not compensate for the lower temperature in providing a good bonding between splats.

Conclusions

Careful selection of deposition parameters can dramatically improve corrosion resistance of HVOF coatings. Morphology of iron-based amorphous coatings has been improved to eliminate speckles of porosity that have a detrimental effect on the corrosion resistance. Splashing of primary feedstock particles is the key mechanism for the speckle formation. However no direct quantitative measurement of the amount of splashed matter was done in the present study. Overall coating porosity

and integrity is a condition that is not necessarily identical to a speckle-free condition, since morphology of some coatings appeared good while the corrosion resistance was poor. Corrosion life of optimized coatings is still to be determined.

References

1. Schroeder, V., C.J. Gilbert, and R.O. Ritchie, *Comparison of the corrosion behavior of a bulk amorphous metal, $Zr_{41.2}Ti_{13.8}Cu_{12.5}Ni_{10}Be_{22.5}$, with its crystallized form.* Scripta Materialia, 1998. 38[10], 1481-1485.
2. Farmer, J.C., et al. *Corrosion characterization of iron-based high-performance amorphous-metal thermal-spray coatings*. 2005. Denver, CO, United States: American Society of Mechanical Engineers, Pressure Vessels and Piping Division (Publication) PVP, 7, American Society of Mechanical Engineers, New York, NY 10016-5990, United States 583-589.
3. Poon, S.J., et al., *Synthesis of iron-based bulk metallic glasses as nonferromagnetic amorphous steel alloys.* Applied Physics Letters, 2003. 83[6], 1131-1133.
4. Lugscheider, E., C. Herbst, and A. Fischer. *Thermal spraying of high performance thermoplastics*. 1998. Nice, France: Proceedings of the International Thermal Spray Conference, 1, ASM International 19-24.
5. Totemeier, T.C., R.N. Wright, and W.D. Swank, *FeAl and Mo-Si-B intermetallic coatings prepared by thermal spraying.* Intermetallics, 2004. 12[12], 1335-1344.
6. Friis, M., C. Persson, and J. Wigren, *Influence of particle in-flight characteristics on the microstructure of atmospheric plasma sprayed yttria stabilized ZrO_2.* Surface & Coatings Technology, 2001. 141[2-3], 115-127.
7. Schwetzke, R. and H. Kreye. *Microstructure and properties of tungsten carbide coatings sprayed with various HVOF spray systems.* 1998. Nice, France: Proceedings of the International Thermal Spray Conference, 1, ASM International 187-192.
8. Moreau, C., P. Cielo, and M. Lamontagne, *Flattening and solidification of thermally sprayed particles.* Journal of Thermal Spray Technology, 1992. 1[4], 317-323.
9. Branagan, D.J., et al., *Wear and Corrosion Resistant Amorphous / Nanostructured Steel Coatings For Replacement of Electrolytic Hard Chromium,* in *International Thermal Spray Conference*. 2006: Seattle.
10. Farmer, J.C., et al., *Corrosion resistance of thermally sprayed high-boron iron-based amorphous-metal coatings: $Fe_{49.7}Cr_{17.7}$ $Mn_{1.9}Mo_{7.4}W_{1.6}B_{15.2}$ $C_{3.8}Si_{2.4}$.* Journal of Materials Research, 2007. 22[8], 2297-2311.
11. Kroupa, F. and J. Dubsky, *Pressure dependence of Young's moduli of thermal sprayed materials.* Scripta Materialia, 1999. 40[11], 1249-1254.
12. Duan, K. and R.W. Steinbrech, *Influence of sample deformation and porosity on mechanical properties by instrumented microindentation technique.* Journal Of The European Ceramic Society, 1998. 18[2], 87-93.
13. Trice, R.W. and K.T. Faber, *Role of lamellae morphology on the microstructural development and mechanical properties of small-particle plasma-sprayed alumina.* Journal of the American Ceramic Society, 2000. 83[4], 889-896.
14. Escure, C., et al., *Visualization of Particle Impact in Thermal Spray*. Proceedings of the International Thermal Spray Conference, ITSC, 2000, 743-752.
15. Farmer, J.C., et al. *Corrosion Resistances of Iron-Based Amorphous Metals with Yttrium and Tungsten Additions in Hot Calcium Chloride Brine: Fe48Mo14Cr15Y2C15B6 and W-*

Containing Variants. in *Background Report – Proceedings 210th Meeting of Electrochemical Society – Cancun, Mexico*. 2006:

This work performed under the auspices of the U.S. Department of Energy by Lawrence Livermore National Laboratory under Contract DE-AC52-07NA27344.